BIOCHEMISTRY
including biophysical chemistry & molecular biology
Article

Biochemistry **2010,** *49,* 9911–9921 9911
DOI: 10.1021/bi100974v

Adaptation to a High-Tungsten Environment: *Pyrobaculum aerophilum* Contains an Active Tungsten Nitrate Reductase[†]

Simon de Vries,[‡] Milica Momcilovic,[§] Marc J. F. Strampraad,[‡] Julian P. Whitelegge,[∥] Ashkan Baghai,[⊥] and Imke Schröder*[,⊥]

[‡]*Laboratory of Biotechnology, Delft University of Technology, Julianalaan 67, 2628 BC Delft, The Netherlands,* [§]*Biomedical Engineering Interdepartmental Program,* [∥]*Department of Chemistry and Biochemistry, and* [⊥]*Department of Microbiology, Immunology, and Molecular Genetics, University of California at Los Angeles, California 90095, United States*

Received June 16, 2010; Revised Manuscript Received September 3, 2010

ABSTRACT: Nitrate reductases (Nars) belong to the DMSO reductase family of molybdoenzymes. The hyperthermophilic denitrifying archaeon *Pyrobaculum aerophilum* exhibits nitrate reductase (Nar) activity even at WO_4^{2-} concentrations that are inhibitory to bacterial Nars. In this report, we establish that the enzyme purified from cells grown with 4.5 μM WO_4^{2-} contains W as the metal cofactor but is otherwise identical to the Mo-Nar previously purified from *P. aerophilum* grown at low WO_4^{2-} concentrations. W is coordinated by a bis-molybdopterin guanine dinucleotide cofactor. The W-Nar has a 2-fold lower turnover number (633 s^{-1}) but the same K_m value for nitrate (56 μM) as the Mo-Nar. Quinol reduction and nitrate oxidation experiments monitored by EPR with both pure W-Nar and mixed W- and Mo-Nar preparations suggest a monodentate ligation by the conserved Asp241 for W(V), while Asp241 acts as a bidentate ligand for Mo(V). Redox titrations of the Mo-Nar revealed a midpoint potential of 88 mV for Mo(V/IV). The E_m for W(V/IV) of the purified W-Nar was estimated to be −8 mV. This relatively small difference in midpoint potential is consistent with comparable enzyme activities of W- and Mo-Nars. Unlike bacterial Nars, the *P. aerophilum* Nar contains a unique membrane anchor, NarM, with a single heme of the o_P type (E_m = 126 mV). In contrast to bacterial Nars, the *P. aerophilum* Nar faces the cell's exterior and, hence, does not contribute to the proton motive force. Formate is used as a physiological electron donor. This is the first description of an active W-containing Nar demonstrating the unique ability of hyperthermophiles to adapt to their high-WO_4^{2-} environment.

Denitrification is an important anaerobic respiratory pathway employed by a diverse group of bacteria and archaea. The four enzymes, Nar, Nir, Nor, and Nos, catalyzing the entirety of this pathway reduce nitrate via nitrite, nitric oxide, and nitrous oxide to dinitrogen gas, respectively (*1*−*5*). The denitrification pathway and the properties of the four enzymes involved have been studied extensively in Gram-negative Proteobacteria, including *Paracoccus denitrificans*, *Paracoccus halodenitrificans*, *Ralstonia eutropha*, *Pseudomonas aeruginosa*, and *Pseudomonas stutzeri*, and are reviewed in refs (*1*−*3*). The pathway is, however, less understood in Gram-positive bacteria and archaea (*2*, *4*−*8*). In contrast to bacterial denitrification enzymes, all four denitrification pathway enzymes in *Pyrobaculum aerophilum* directly couple to the quinone pool (*4*, *5*, *7*). With the exception of nitrate reductases and quinol:NO reductases, bacterial denitrification enzymes use periplasmic *c*-type cytochromes or blue copper proteins as electron donors (*1*−*3*). In bacteria, these electron donors are reduced by the electrogenic cytochrome bc_1 complex, producing an overall H^+/e stoichiometry of 1 for the complete reduction of nitrate to dinitrogen gas from quinol (*2*).

The first step of the bacterial denitrification pathway, catalyzed by the membrane-bound NarGHI-type nitrate reductase (Nar),[1] is directly coupled to the generation of a proton motive force to sustain cell growth. The NarGHI-type Nar is largely conserved among all nitrate respiring bacteria and archaea (*9*−*11*). The enzyme has been extensively studied in mesophilic nitrate reducing bacteria such as the ammonifier *Escherichia coli* and the denitrifiers *Pa. denitrificans*, *Ps. stutzeri*, *Pseudomonas denitrificans*, and others (*10*, *11*). The *E. coli* NarGHI enzyme has been recently crystallized and serves as the prototype in our understanding of the structure and function of nitrate reductases in other bacteria (*12*, *13*). The quaternary structure of NarGHI is a dimer of heterotrimers. The largest subunit of the heterotrimer is the 139 kDa NarG, which contains a Mo-bis-MGD and a single [Fe-S] center (FS0). The 58 kDa NarH subunit harbors four distinct [Fe-S] centers, three [4Fe-4S] centers (FS1, FS2, and FS3), and one

[†]This work was supported by grants from the National Science Foundation (MCB-0345037) to I.S. and The Netherlands Organization for Scientific Research (NWO 700.54.003) to S.d.V.

*To whom correspondence should be addressed: Department of Microbiology, Immunology, and Molecular Genetics, UCLA, BSRB, RM 290, 615 Charles E. Young Dr. S., Los Angeles, CA 90095. Phone: (310) 206-0319. Fax: (310) 267-2774. E-mail: imkes@microbio.ucla.edu.

[1]Abbreviations: Nar, nitrate reductase; Nir, nitrite reductase; Nor, NO reductase; Nos, N_2O reductase; BV, benzyl viologen; MV, methyl viologen; PB, plumbagin; W-Nar, tungsten-containing Nar; Mo-Nar, molybdenum-containing Nar; DMSO reductase, dimethyl sulfoxide reductase; TMAO reductase, trimethylamine *N*-oxide reductase; FDH, formate dehydrogenase; MQ, menaquinone; pmf, proton motive force; bis-MGD, bis-molybdopterin guanine dinucleotide; GMP, guanosine monophosphate.

© 2010 American Chemical Society
Published on Web 09/23/2010

[3Fe-4S] center (FS4). The 26 kDa NarI hydrophobic subunit accommodates a diheme *b*. NarI serves as the membrane anchor for NarGH and mediates the transfer of electrons from the quinol pool across the membrane to the [Fe-S] centers in NarH and subsequently to the Mo active site in NarG according to the $QH_2 \rightarrow b_D \rightarrow b_P \rightarrow$ FS4 $\rightarrow$ FS3 $\rightarrow$ FS2 $\rightarrow$ FS1 $\rightarrow$ FS0 $\rightarrow$ Mo-bis-MGD $\rightarrow NO_3^-$ pathway (*12*).

To date, few archaeal Nars have been characterized. A three-subunit Mo-containing Nar was isolated from *P. aerophilum* (*14*), and two-subunit NarGH-type enzymes were purified from the halophilic archaea *Haloarcula marismortui* and *Haloferax mediterranei* (*15*−*17*). A distinctive feature of the *H. marismortui* and *Ha. mediterranei* nitrate reductases is their outward-facing active site (*16*, *18*). In contrast, all bacterial nitrate reductases of the NarGHI type face the cell's interior and catalyze nitrate reduction in the cytoplasm (*11*, *19*). An additional interesting feature of archaeal Nars is the apparent absence of a *narI*-type gene encoding the membrane anchor subunit found in bacterial Nars and thus raises the question of how archaeal Nars are bound to the membrane.

Recently, Yoshimatsu et al. purified a cytochrome *b*-561, NarC, from membranes of *H. marismortui* (*20*). On the basis of gene clustering of *narC* with *narGH* and homology to the bc_1 complex cytochrome *b*, the authors suggested that in *H. marismortui* NarGH may form a respiratory supercomplex with the bc_1 complex. Martinez-Espinosa et al. have proposed that two genes flanking *narGH* in *Ha. mediterranei* may serve to anchor the enzyme to the cytoplasmic membrane and directly accept electrons from an associated bc_1 complex (*18*).

Nitrate respiration at high temperatures presents a challenge; typical high-temperature environments are enriched with tungstate but depleted of molybdate (*21*). Because of its similar chemistry, WO_4^{2-} usually acts antagonistically to MoO_4^{2-}. In the presence of WO_4^{2-}, bacteria cannot assemble an active Nar (*22*, *23*). The hyperthermophile *P. aerophilum* is a denitrifying archaeon requiring WO_4^{2-} for growth (*6*). Afshar et al. demonstrated that the external WO_4^{2-} concentration affects the denitrification pathway efficiency of this archaeon, resulting in complete denitrification only at high WO_4^{2-} concentrations. Nar purified from *P. aerophilum* grown with MoO_4^{2-} and a limiting WO_4^{2-} concentration (0.5 μM) was shown to contain Mo as a metal cofactor and a heme *b* membrane anchor (*14*).

We report here that the Nar purified from *P. aerophilum* grown in the absence of added MoO_4^{2-} and with 4.5 μM WO_4^{2-} is a W enzyme. The W-Nar is identical to the Mo-Nar, indicating that either metal can serve as the active site ion. W is coordinated by bis-molybdopterin guanine dinucleotide (W-bis-MGD). The heme *b* was further characterized and identified as heme o_P. Heme o_P is coordinated by a membrane anchor, NarM, a homologue of one the proteins suggested to associate with the membrane of *Ha. mediterranei* Nar (*18*). The *narM* gene is conserved in all archaeal Nar operons identified thus far, and its gene product is related to electron transfer subunits of bacterial, periplasmic oxidoreductases. This is the first documentation of an active W-Nar and presents fascinating insight into how hyperthermophiles adapt to the metal composition of their environment. The coordination of tungsten as well as evolutionary and bioenergetic implications is discussed.

EXPERIMENTAL PROCEDURES

Growth Conditions. *P. aerophilum* (DSM 7523) was cultured in a marine medium at 95 °C under anaerobic conditions as previously described (*6*) but with 4.5 μM Na_2WO_4 and the following modifications: NaBr, $SrCl_2 \cdot 6H_2O$, NaF, KI, and $Na_2MO_4 \cdot 2H_2O$ omitted from the medium. For the purification of the W/Mo-Nar, *P. aerophilum* was cultured with 1 μM Na_2WO_4 and 0.5 μM Na_2MoO_4. For large scale culture, *P. aerophilum* was grown in 70 L of medium in a 100 L glass-lined fermentor (Pfaudler). Growth was monitored by measurement of the optical density at 600 nm. Cells were harvested in the late exponential growth phase at an A_{600} of 0.28−0.32. After being harvested by concentration with a hollow-fiber filter (A/G Technology), cells were centrifuged for 40 min at 15000*g* and stored at −80 °C.

Purification of Nitrate Reductase. The enzyme purification procedure was performed under aerobic conditions and at 4 °C unless indicated otherwise. All buffers contained 0.5 mM phenylmethanesulfonyl fluoride (PMSF). Initial purification steps, including HiTrapQ Sepharose chromatography, were performed essentially as previously described by Afshar et al. (*14*) with the following modifications. Cell lysis was enhanced by French press treatment, and membrane-bound protein was extracted using 3% Triton X-100. While the first chromatography step was essentially as described, enzyme purification was improved by employing a second HiTrapQ Sepharose (Pharmacia) chromatography step using 20 mM Tricine (pH 7.6) with 0.2% Triton X-100 as the buffer and a 0 to 0.3 M NaCl gradient, in which nitrate reductase eluted with ~70 mM NaCl. Following a protein concentration step with Centricon-100 concentrators (Amicon), protein was separated on a Superdex 200 column (Pharmacia) using 20 mM Tricine (pH 7.6), 0.05% Triton X-100, and 0.15 M NaCl. Nitrate reductase fractions were combined, concentrated, and stored at 4 °C and for the long term at −80 °C.

Analytical Protein Assays. Nitrate and nitrite reductase activities were assayed anaerobically at 75 °C using reduced benzyl viologen (BV) or methyl viologen (MV) as the electron donor as previously described (*14*). In addition, nitrate reductase activity was assayed with reduced plumbagin as the electron acceptor (*8*). Succinate dehydrogenase activity was measured in the reverse direction with reduced benzyl viologen as the electron donor essentially as described elsewhere except that the assay was performed at 75 °C (*24*). Malate dehydrogenase activity was measured at 75 °C with NAD^+ as the electron acceptor as described previously (*24*). Formate dehydrogenase activity was measured anaerobically and at 75 °C with methylene blue and dimethyl menaquinone (DMN) as described in ref *24*. One unit of enzyme activity is defined as 1 mmol of substrate (nitrate, nitrite, fumarate, formate, or malate) reduced or oxidized per minute. The qualitative electron donor screen was performed anaerobically and at 80 °C in capped serum vials with *P. aerophilum* membrane fractions. The assay contained 50 mM phosphate buffer (pH 7.0), 10 mM sodium nitrate, and the following sodium salts at 50 mM: formate, acetate, tartrate, DL-malate, pyruvate, DL-lactate, and succinate. In addition, NADH and NADPH at 10 mM and 0.1% casamino acids were tested as potential electron donors. After 15 min, the reaction was stopped when the vials were transferred to ice. The membrane fraction was removed by centrifugation, and nitrite formation was assessed with sulfanilamide and *N*-(1-naphthyl)ethylenediamine (*24*). The protein concentration was determined with the DC Bio-Rad protein assay (Bio-Rad) using bovine serum albumin (Sigma) as the standard.

Iron, Mo, and W were quantified by inductively coupled plasma mass spectrometry at the Soil and Plant Analysis Laboratory of the University of Wisconsin/Extension (Madison, WI).

Pyridine hemochrome analysis was conducted as described previously (*8*).

N-Terminal amino acid sequencing was performed with the protein obtained after the last purification step. Protein was incubated with SDS Laemmli buffer for 1.5 h at 90 °C and separated by sodium dodecyl sulfate−polyacrylamide electrophoresis (SDS−PAGE) using 4 to 12% Bis-Tris gels (NuPAGE, Invitrogen). Protein was subsequently transferred to a polyvinylidene difluoride membrane (PVDF, Bio-Rad). Sequencing was conducted at the Microchemical Core Facility of the Keck School of Medicine at the University of Southern California/Norris Comprehensive Cancer Center.

Guanine Identification and Characterization. To characterize the metal pteridin cofactor, guanine analysis was performed essentially as described by Hilton and Rajagopalan (*25*). To release the cofactor, purified nitrate reductase was hydrolyzed by addition of 0.1 M HCl and subsequent incubation at 100 °C for 1 h. The sample was cooled to room temperature, and the pH was adjusted to 8.5 with 1 M NaOH. The centrifuged sample was applied to a 4.1 mm × 300 mm Versapack 10 μm C-18 reverse-phase HPLC column (Alltech) equilibrated with 50 mM ammonium acetate and 7% methanol at a flow rate of 1 mL/min. The absorbance was monitored at 280 nm with a Shimadzu UV detector. Guanine was identified by retention time on the HPLC column and characteristic UV−vis spectrum compared to those of a standard (Sigma). For quantification, the integrated area of the absorbance peak associated with the eluting compound was calculated. It was compared to a calibration curve generated from guanine standards.

Mass Spectrometry. Nar subunits were separated via SDS−PAGE. Protein bands corresponding to NarG and NarM were excised, treated with trypsin, and analyzed by LC−MS/MS (liquid chromatography and tandem mass spectroscopy) essentially as described by Shevchenko et al. (*26*).

For heme identification, hemes were extracted according to the procedure from Lübben and Morand (*27*). Extracted hemes were analyzed by size exclusion chromatography and electrospray ionization mass spectrometry (SEC−MS) as described previously (*28*). A sizing column (Super SW 2000, 4.6 mm × 300 mm, 40 °C Tosoh Biosep) was equilibrated in a chloroform/methanol/1% formic acid mixture in water (4:4:1, v/v/v) at a rate of 250 μL/min prior to injection of the extracted heme sample (100 μL). The orifice potential (65 V) used was typical of values employed for protein ionization.

EPR Spectroscopy and Redox Titrations. EPR spectra were recorded with a Varian E-9 spectrometer at X-band frequency equipped with a home-built helium flow system (*29*). Sample reduction and reoxidation were conducted anaerobically via incubation for 1 min at 40 °C with 1.0 mM plumbagin (PBH_2) and 1.5 mM KNO_3, respectively. The pH of purified Nar EPR samples was adjusted by addition of small aliquots of 0.5−1.0 M buffers to give a final concentration of 0.1 M (MES at pH 6, MOPS at pH 7, and Tris at pH 8). Membranes adjusted to various pH values were washed three times in one of these three buffers at 0.1 M. Dye-mediated redox titrations (oxidative and reductive) monitored by EPR spectroscopy were performed in the additional presence of 0.1 M NaCl and with each of the following dyes at 80 μM: PES (phenazine ethosulfate), PMS (phenazine methosulfate), DCIP (2,6-dichlorophenolindophenol), methylene blue, resorufine, indigo carmine, 2-hydroxy-1,4-naphthaquinone, anthraquinone 2-sulfonate, phenosafranin, safranin, neutral red, benzyl viologen, and methyl viologen. Dye-mediated redox titrations monitored by UV−vis spectroscopy were conducted in the presence of 20 μM PMS, PES, 2-hydroxy-1,4-naphthaquinone, anthraquinone 2-sulfonate, and 40 μM duroquinone. Midpoint potentials are quoted versus the normal hydrogen electrode (NHE) and were measured with a Pt electrode using saturated Ag/AgCl as a reference electrode; the redox potential was varied via addition of concentrated aliquots of sodium dithionite or ferricyanide. Dye-mediated redox titrations were conducted anaerobically in a Coy anaerobic chamber. The Nernst equation was used to calculate the midpoint potentials. Quoted midpoint potentials are ±10 mV, except for FS3 (±20 mV). Simulation of EPR spectra was performed with a home-written program for the Macintosh computer operating under OS 9.2.2.

RESULTS

Purification of Nitrate Reductase from Cells Grown with 4.5 μM WO_4^{2-} without Added MO_4^{2-}. Unlike bacteria, *P. aerophilum* maintains an active nitrate reductase (Nar) even when grown at WO_4^{2-} concentrations as high as 5 μM (*6*). Nar from *P. aerophilum* cultured with MO_4^{2-} and under WO_4^{2-} concentration-limiting conditions (0.5 μM) was previously purified and shown to contain Mo in addition to Fe as metal cofactors (*14*). The purpose of this study was to examine the cofactor composition and kinetic properties of Nar from cells grown at high WO_4^{2-} concentrations. *P. aerophilum* was grown anaerobically with nitrate in a medium containing 4.5 μM WO_4^{2-} but without added MoO_4^{2-}. During initial purification attempts, we noticed that Nar from cells grown at high WO_4^{2-} concentrations appeared to be more labile than the previously isolated Mo-Nar; i.e., the enzyme gradually lost activity (*14*). Therefore, the purification procedure was modified to prevent enzyme inactivation. One of the modifications was the omission of hydroxyapatite chromatography known to delipidate membrane proteins, which resulted in an irreversible aggregation of Nar with concomitant loss of activity. Many tungsten-containing enzymes are inactivated by oxygen (*21*). We, therefore, attempted purification of Nar with N_2-flushed buffers and in the presence of 5 mM dithiothreitol (DTT). However, DTT caused the complete loss of enzyme activity, and N_2-flushed buffers did not increase Nar stability.

Nar was purified by two anion exchange chromatography steps and one size exclusion chromatography step (Table S1 of the Supporting Information). After the final chromatography step, the enzyme was enriched 24-fold as compared to the membrane fraction with a purity of 80% approximated by SDS−PAGE (data not shown). Nar purity is consistent with the cofactor composition summarized in Table 1. Purified Nar has a subunit composition identical to that of the enzyme that was purified from cells grown at 0.5 μM WO_4^{2-}, i.e., 130, 52, and 32 kDa (*14*).

Subunit Identification and Operon Organization. The N-terminal sequence of the 52 kDa subunit was determined to be MNVRAQITMAMNLDK, which corresponds to the sequence predicted by the *P. aerophilum narH* gene. However, the N-terminal sequence of the 130 kDa subunit was blocked, and attempts to obtain the N-terminal sequence for the smallest subunit were unsuccessful. Therefore, the 130 and 32 kDa subunits were digested with trypsin within the SDS−polyacrylamide gel, extracted, and subjected to mass spectrometry analysis. Masses for 17 distinct peptides were obtained from the 130 kDa subunit, including YTDLPFLVILEPAGDGTYLQGR identifying NarG. The 29

Table 1: Cofactor Composition and Kinetic Parameters of *P. aerophilum* Nars

cofactor	W-Nar (mol/mol)	Mo-Nar[a] (mol/mol)
W	0.55	0.06
Mo	< 0.01	0.8
non-heme Fe	17.6	15.4
GMP	1.71	[b]
heme o_p	0.72	0.49

kinetic parameter	W-Nar	Mo-Nar
K_M (μM)	56	58
$k_{cat}(BV_{red} \rightarrow NO_3)$ (s^{-1})	633	1162
$k_{cat}(PBH_2 \rightarrow NO_3^-)$ (s^{-1})	62	116

[a]Data from ref *14*. [b]Not determined in this work or in ref *14*.

masses for the 32 kDa subunit sample included AGFGAENLVAGAGYGLNPQQR and identified a hypothetical conserved protein encoded by a gene downstream of *narH* (Figure 1A). We suggest that the 32 kDa peptide represents the membrane anchor to the NarGH subunits of the archaeal Nar and hence call it NarM for nitrate reductase membrane anchor. Thus, the protein composition of the Nar purified from *P. aerophilum* grown with 4.5 μM WO_4^{2-} is identical to that of the Mo-containing enzyme previously isolated from cells grown with 0.5 μM WO_4^{2-}, consistent with the presence of only one *narGHM* operon in the *P. aerophilum* genome (*14*).

While the *P. aerophilum* NarG and NarH subunits are 47−55% identical to the respective proteins from *E. coli*, *Thiosphaera pantropha*, and *Bacillus subtilis*, NarM exhibits no homology to the NarI membrane anchor of the bacterial nitrate reductases. However, NarM-like proteins are conserved in all archaeal nitrate reductase operons identified thus far with high similarity probability values ranging from 7×10^{-56} to 10^{-103} among *Aeropyrum pernix* and other *Pyrobaculum* species, and 10^{-14} for haloarchaea (Figure 1A). NarM homologues are also related to the γ subunits of periplasmic oxidoreductases, such as EbdC of the *Aromatoleum aromaticum* strain EbN1 ethylene benzene dehydrogenases and SerC of the *Thauera selenatis* selenate reductase (E-value = 2×10^{-10}) (Figure 1B) (*18*, *30*). Both subunits were shown to bind heme *b* (*31*, *32*).

A gene encoding the putative private chaperone, *narJ*, known to be essential for the assembly of active bacterial Nars (*33*−*35*), is transcribed divergently from the *P. aerophilum narG* gene (Figure 1A). The *narJ* gene is part of or in the direct vicinity of other archaeal *narGHM* putative operons with the exception of *Pyrobaculum arsenaticum*, where it is located elsewhere on the chromosome.

Cofactor Analysis. Inductively coupled plasma mass spectroscopy was used to determine the total metal content of nitrate reductase. The enzyme preparation contained W, but Mo was not detected (Table 1). This suggests that the purified Nar is a W-containing enzyme, and it is in this respect distinct from all other Nars that have been characterized thus far (*10*, *11*, *14*). The amount of iron determined was consistent with the presence of one [3Fe-4S] center and four [4Fe-4S] centers (Table 1).

Cofactors that coordinate Mo and W in different enzymes exhibit considerable variability, in both structure and number (*36*, *37*). Nar belongs to the dimethyl sulfoxide (DMSO) reductase family of molybdo enzymes containing a Mo-bis-MGD cofactor (*10*). To determine the type and number of pterin cofactor molecules in the *P. aerophilum* Nar, the cofactor was extracted and its nucleotide was released by acidic denaturation of the protein.

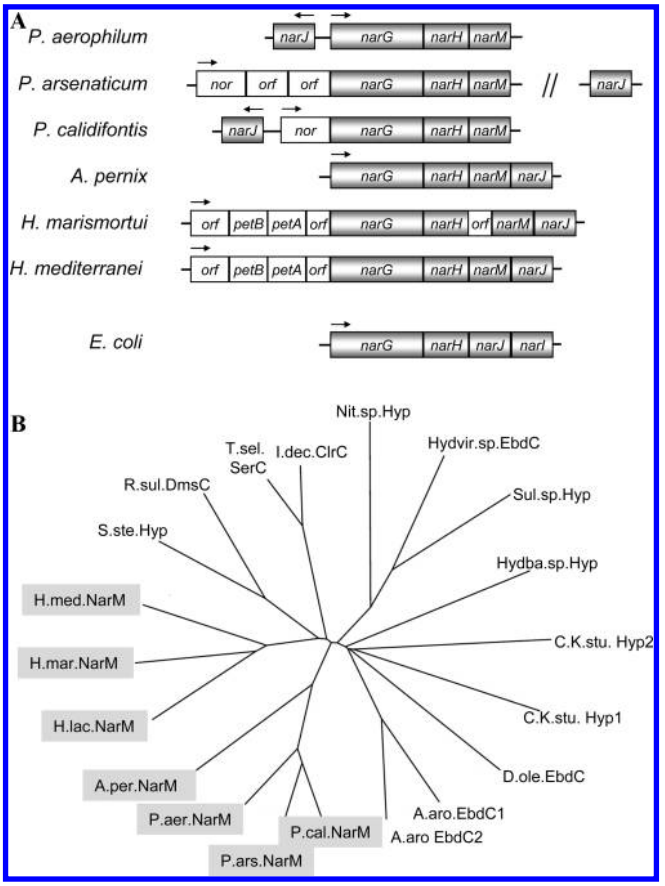

FIGURE 1: Organization of archaeal and *E. coli* Nar operons (A) and phylogenetic comparison of archaeal NarMs and bacterial γ subunits of periplasmic oxidoreductases (B). (A) Genes *petA* and *petB* encode the Rieske protein and cytochrome *b* of the bc_1 complex, respectively. (B) Archaeal NarMs are shaded; abbreviations for bacterial enzyme γ subunits are as follows: DsmC, dimethyl sulfide dehydrogenase; SerC, selenate reductase; ClrC, chlorate reductase; EbdC, ethylbenzene dehydrogenase; and Hyp, hypothetical. Other abbreviations: P.aer, *P. aerophilum*; P.ars, *Pyrobaculum arsenaticum*; P.cal, *Pyrobaculum calidifontis*; A.per, *Aeropyrum pernix*; H.lac, *Halorubrum lacusprofundi*; H.med, *Ha. mediterranei*; H.mar, *H. marismortui*; S.ste, *Sagittula stellata* E-37; R.sul, *Rhodobacter sulfidophilus*; T.sel, *Thauera selenatis*; I.dec, *Ideonella dechloratans*; Nit.sp., *Nitratiruptor* sp. strain SB155-2; Hydvir. sp., *Hydrogenivirga* sp. 128-5-R1-1; Sul.sp., *Sulfurihydrogenibium* sp. YO3AOP1; Hydba.sp., *Hydrogenobaculum* sp. Y04AAS1; C.K.stu, *Candidatus Kuenenia stuttgartiensis*; D.ole, *Desulfococcus oleovorans* Hxd3; A.aro, *Aromatoleum aromaticum*.

On the basis of its UV−vis spectrum and sample retention time in reverse-phase HPLC as compared to those of a standard, guanine was identified as the nucleotide attached to pterin and the concentration of the extracted guanine was consistent with two MGDs per W (Table 1).

Kinetic Characterization of W-Nar. The specific activity of the W-Nar was determined using reduced benzyl viologen as the electron donor. The enzyme exhibited a V_{max} of 47 units/mg and a K_m for nitrate of 56 μM. On the basis of the amount of tungsten present in the preparation, a turnover number (k_{cat}) of 633 s^{-1} was calculated (Table 1). The activity of the W-Nar is inhibited 95 and 92% by 2 mM sodium azide and 2 mM sodium cyanide, respectively, similar to the Mo-Nar (*14*). Nar activity was also assayed in membrane fractions expressing either W-Nar or Mo-Nar using reduced BV or the reduced form of the menaquinone analogue plumbagin as the electron donor. The k_{cat} values obtained with PBH_2 were ~10-fold smaller as compared to the activities determined with reduced

Table 2: Determination of the Active Site Orientation of Nar

addition	Nar $MV_{red} \rightarrow NO_3^-$ (units/mg)	Nar $BV_{red} \rightarrow NO_3^-$ (units/mg)	Nir $BV_{red} \rightarrow NO_2^-$ (unit/mg)	SDH $BV_{red} \rightarrow$ fumarate (units/mg)	MDH malate $\rightarrow NAD^+$ (unit/mg)
none	3.87	4.81	0.92	< 0.05	< 0.05
lauryl maltoside[a]	3.87	4.03	0.74	1.80	0.19

[a]Added to give a final concentration of 0.2%.

benzyl viologen as the electron donor for both types of Nars (Table 1).

To gain insight into a possible electron donor for nitrate reductase, we performed an end point assay screen with the *P. aerophilum* membrane fraction, nitrate, and various potential electron donors. The electron donors included casamino acids, formate, acetate, tartrate, DL-malate, pyruvate, DL-lactate, succinate, NADH, and NADPH. The activity was determined by measuring the formation of nitrite after incubation for 15 min at 80 °C. Significant accumulation of nitrite was only detectable in assays containing formate. Subsequently, formate dehydrogenase activity was determined in the membrane fraction at 75 °C with methyl blue and the menaquinone analogue dimethyl menaquinone (DMN) as electron acceptors to be 1.2 units/mg and 0.5 unit/mg, respectively. Thus, formate donates an electron to nitrate reductase.

Orientation of the Nar Active Site. Haloarchaeal Nars have been demonstrated to face the cell's exterior (*16*, *18*). This cellular orientation is in contrast to all bacterial NarGHI-type nitrate reductases, whose active site faces the cytoplasm (*10*). To examine whether an outward orientation is a commonality of archaeal nitrate reductases, we determined the cellular orientation of the *P. aerophilum* Nar using the membrane-impermeable methyl viologen (MV) and benzyl viologen radical (BV) as electron donors (Table 2) (*18*, *38*). Nitrate reductase activity was maximal in intact cells without stimulation by the addition of lauryl maltoside, supporting the notion that the Nar active site faces the exterior of *P. aerophilum*. An outward orientation was confirmed for nitrite reductase, which commonly assumes this orientation in denitrifying bacteria (*11*). Cell intactness was ensured by determination of the activities of two intracellular enzymes, succinate dehydrogenase and malate dehydrogenase. The observation that succinate dehydrogenase activity, assayed as BV:fumarate reductase, was detectable in whole cells only when cells were permeabilized with detergent further indicates that BV is impermeable to *P. aerophilum* membranes.

Heme Identification by Mass Spectrometry. The identity of the previously identified Nar-associated heme *b* (*14*) was further characterized to be of the o_P type using size exclusion chromatography and mass spectroscopy [SEC−MS (Figure S1 of the Supporting Information)]. Nar contains a heterogeneous mixture of hemes o_{P1} and o_{P2} in a 0.3:0.7 ratio. Hemes o_{P1} and o_{P2} are hydrophobic heme *b* derivatives with ethenylprenyl and hydroxyethylgeranylgeranyl side chains, respectively (*27*). Pyridine hemochrome analysis was used to estimate the concentration of heme o_P to be 16.7 μM per 23.25 μM enzyme complex extrapolating to one heme o_P per Nar complex (Table 1). This value differs from those of all bacterial nitrate reductases that are known to contain two heme *b* molecules per Nar complex (*10*, *39*−*41*). Dye-mediated redox titrations monitored optically with the purified W-Nar yielded a single midpoint potential of 126 mV for heme o_P (Figure S2 of the Supporting Information and Table 3).

Table 3: Midpoint Potentials of Nar [Fe-S] Centers and the W and Mo Cofactors[a]

	E_m for *P. aerophilum* Nar (mV)	E_m for *E. coli* Nar (mV)
W(V/IV)	−8[b]	
Mo(V/IV)	88[c]	90[d]
FS4	−120[e]	180[f]
FS3	−150[e]	−55[f]
FS2	←483[e]	−420[f]
FS1	−1[e]	130[f]
FS0	not detected	−55[g]
heme o_p	126[e]	
heme b_D		20[h]
heme b_P		120[h]

[a]All data for the *P. aerophilum* Nar were obtained using the copurified W-Nar and Mo-Nar, except for the Mo(V) potential, which was determined using membranes. Note that in the dye-mediated redox titrations the Mo or W cofactor of the *P. aerophilum* Nar is lost; hence, the midpoint potentials of the [Fe-S] centers and heme o_p apply to the apo-Nar from *P. aerophilum*. Estimated errors in E_m are ±10 mV. [b]Calculated from the extent of reduction by PBH_2 (see Figure 3) and valid for pH 6; estimated error in E_m of ±15 mV. [c]pH-independent for pH 6 and 8. [d]pH-dependent (90 mV at pH 8.1 and 200 mV at pH 5.85) (*42*, *43*). [e]E_m values for the [Fe-S] centers are at pH 8 and heme o_p at pH 7.4. [f]From refs *43* and *45*. [g]From ref *44*. [h]From refs *39* and *63*.

Characterization of Nitrate Reductase by EPR Spectroscopy. EPR spectroscopy of the purified W-Nar revealed an axial signal (g_z = 2.04, and $g_{x,y}$ = 1.97) for FS4, the oxidized [3Fe-4S] center (Figure 2A and Table 4). After addition of the menaquinone analogue plumbagin (PBH_2), FS4 remained largely oxidized, suggesting that the midpoint potential of this center is more negative than that of plumbagin [E_m(pH 8) = −100 mV]. FS4 was fully reduced with dithionite. Reduction with PBH_2 gave rise to additional signals that were more pronounced after addition of dithionite (*g* values of 2.06, 2.02, 1.95, 1.88, and 1.86) (Figure 2A). These signals are likely due to magnetically interacting [4Fe-4S] centers, specifically FS3 and FS1 (*40*−*43*). The reduced [Fe-S] centers were completely reoxidized by nitrate. The broad EPR signal seen in *E. coli* Nar (*42*, *43*) resulting from the reduction of the very low potential FS2 was not detected, not even at redox potentials of −483 mV (i.e., in the titrations shown in Figure 5). Resonances around g = 5 indicative of center FS0 were also not observed, probably because of the low concentration of Nar used in our experiments (*44*). Furthermore, EPR signals for W(V) in the W-Nar preparation were absent under the experimental conditions used, i.e., at pH 8.

To examine the EPR properties of the heme cofactor, we recorded spectra in the lower magnetic field range and revealed two predominant peaks (Figure 2B). The g = 4.28 feature is due to a small amount of contaminating iron. The g_z = 3.31 peak stems from a low-spin heme center, which is reduced by plumbagin and reoxidized by nitrate. This spectrum differs from that of the *E. coli* Nar, where the two hemes generate two distinct EPR signals [g_z = 3.76, and g_z = 3.36 (*39*−*41*)]. Quantitative analysis of the *P. aerophilum* Nar EPR spectra yielded a

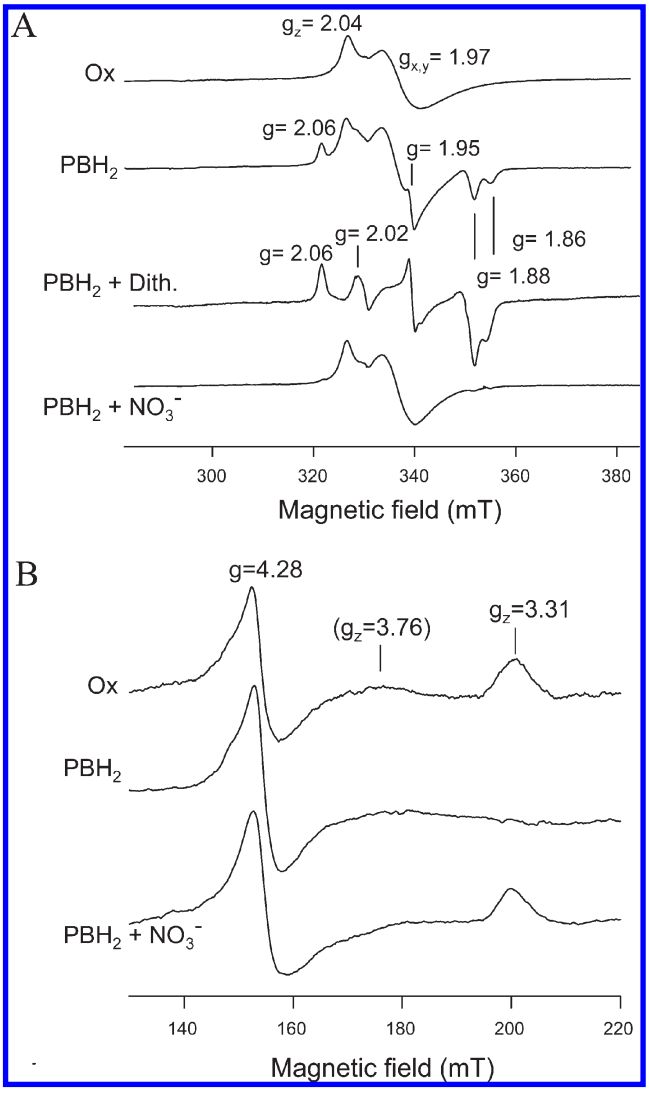

FIGURE 2: X-Band EPR spectra recorded with purified W-Nar showing signals for the [Fe-S] centers (A) and heme o_p (B): Ox, enzyme as isolated (23 μM at pH 8); PBH_2, enzyme after addition of 1 mM reduced plumbagin; PBH_2 + Dith, enzyme after the further addition of a few grains of solid sodium dithionite; $PBH_2 + NO_3^-$, PBH_2-reduced sample in the second trace (in panels A and B) thawed and incubated with 1.5 mM nitrate. The g values of the various [Fe-S] centers are indicated. In panel B, the g_z of 3.76 refers to the position of a second heme (heme b_P) present in the *E. coli* Nar (*63*, *64*). EPR conditions: microwave power, 2 mW; modulation amplitude, 1.0 mT; temperature, 10 K; frequency, 9.25 GHz.

Table 4: EPR Properties of W(V) and Mo(V) Cofactors

	W(V)[a,b]	Mo(V)[b]
g_z, g_y, g_x	1.996, 1.981, 1,958	1.955, 1.980, 1.985
g_{av}	1.978	1.977
H^+ A_z, A_y, A_x (mT)	1.1, 0.9, 1.0	no proton
^{183}W A_z, A_y, A_x (mT)	4.0, 4.0, 2.0	
$^{95,97}Mo$ A_z, A_y, A_x (mT)		0, 0, 5.0
maximal W(V) or Mo(V)	0.11 ± 0.02 $W(V)/W_{total}$	0.35 ± 0.02 $Mo(V)/Mo_{total}$

[a]W-Nar was purified from *P. aerophilum* grown with 4.5 μM W. [b]Data from the W/Mo-Nar purified from *P. aerophilum* grown with 1 μM WO_4^{2-} and 0.5 μM MoO_4^{2-}.

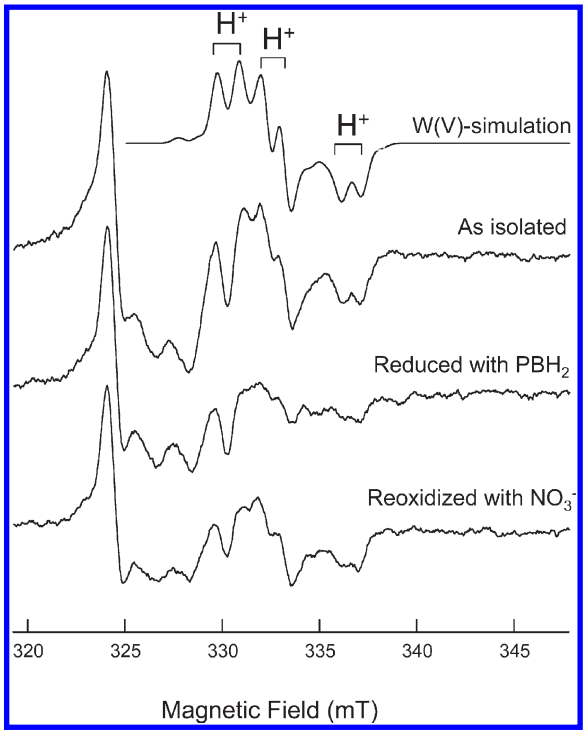

FIGURE 3: X-Band EPR spectra of purified W-Nar displaying the W(V) center. A spectral computer simulation (top trace) of the W(V) signal using fitting parameters indicated in Table 3. The W-Nar concentration was 23 μM at pH 6; the enzyme was reduced and oxidized as described in the legend of Figure 4. The superhyperfine splitting due to magnetic interaction with a nearby proton is indicated by bars and H^+ in the top trace. EPR conditions: microwave power, 2 mW; modulation amplitude, 0.5 mT; temperature, 40 K; frequency, 9.25 GHz.

stoichiometry of 0.8−0.9 heme per [3Fe-4S] center. The amount of heme is consistent with the pyridine hemochrome analysis and supports our finding that the *P. aerophilum* Nar contains only one heme per enzyme complex.

Characterization of the W and Mo Cofactors by EPR. While EPR signals for W(V) were absent at pH 8, signals could be readily detected when the purified enzyme was placed at pH 6 (Figure 3, as isolated). Apparently, the enzyme as isolated is partially reduced. The effect of pH was found to be reversible (data not shown). The W(V) signal of Nar closely matched the simulated W(V) form as a rhombic species with three characteristic g values of <2. The simulation also included a magnetic superhyperfine interaction with a nearby proton resulting in a splitting of each of the three resonances into two (Figure 3 and Table 4). The proton superhyperfine interaction of the W(V) species in the *P. aerophilum* Nar is similar in magnitude to that of the Mo(V) form in the *E. coli* Nar, which is also known to interact with a nearby solvent exchangeable proton with a pK_a value of 7.4 (*45*).

The W cofactor in the *P. aerophilum* Nar can be reduced by PBH_2; approximately 60% of the W(V) form is reduced to the EPR-silent W(IV) form. Addition of nitrate yields approximately 75% of the amount of W(V) present in the as isolated enzyme. The observation that plumbagin cannot completely reduce W(V) to W(IV) suggests that the midpoint potentials of the quinol (E_m for plumbagin of 20 mV at pH 6) and the W cofactor are similar (Table 3). The relatively strong signal in the EPR spectrum at a lower magnetic field shown in Figure 3 is due to a low-spin hexacoordinated Fe^{2+}−NO complex, originating from the ferrous iron of hemes o_{P1} and o_{P2}. A similar heme b Fe^{2+}−NO complex was observed previously in the *E. coli* Nar (*42*).

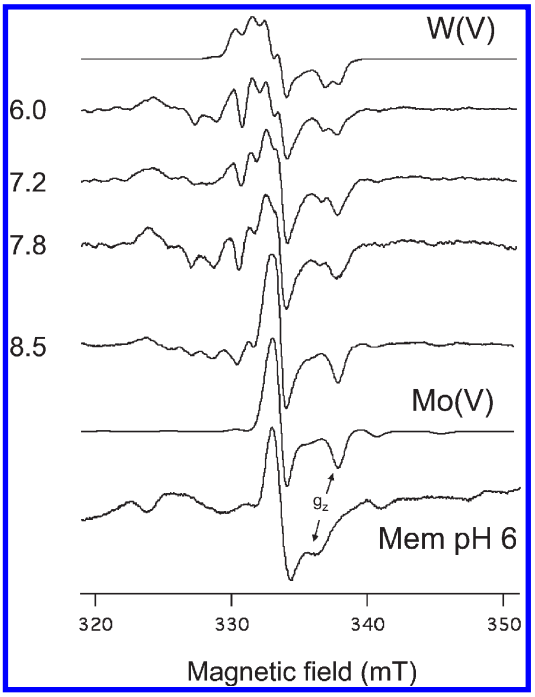

FIGURE 4: X-Band EPR spectra of a purified mixed W/Mo-Nar preparation showing signals from both W(V) and Mo(V). Nar as isolated (15 μM) was incubated with different buffers to vary the pH to the values indicated. Traces labeled W(V) and Mo(V) are spectral computer simulations of the W(V) and Mo(V) signals, respectively. The bottom spectrum was recorded in membranes at pH 6 and displays the unsplit Mo(V) signal; the signal is identical in membranes poised at pH 8 (not shown). The g_z value is shifted to a lower magnetic field (arrow) with respect to the signal in the purified Nar. EPR conditions as described in the legend of Figure 3.

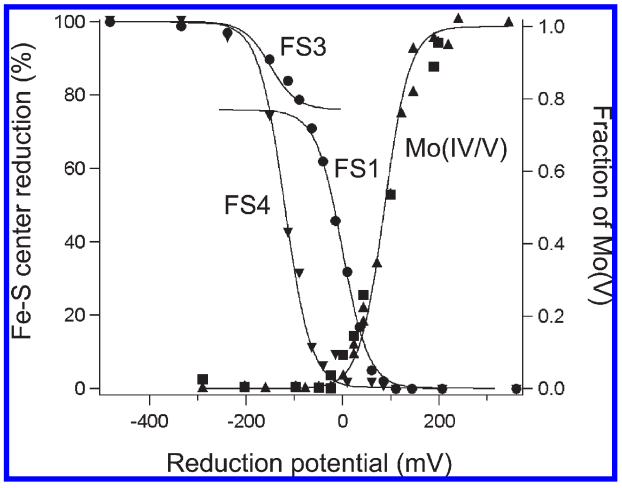

FIGURE 5: Dye-mediated redox titrations. Midpoint potentials of [Fe-S] centers were determined in solubilized, copurified W- and Mo-Nars (pH 7.4), or for Mo(V) (pH 6 or 8) in membranes. The lines are fitted to the Nernst equation (n = 1), and the midpoint potentials are listed in Table 3. The amount of FS4 (▼) was calculated from the g_z = 2.04 peak intensity and from the intensity of the $g_{x,y}$ line. The g = 1.88 and 1.86 resonances (see Figure 4) showed a biphasic titration behavior (●) also observed for *E. coli* Nar (*42*); the relative contributions of FS3 (24%) and FS1 (76%) to these resonances were taken to be the same as that for the *E. coli* enzyme (*42*). Mo(V) data at pH 6 (■) and pH 8 (▲) were fitted to the same Nernst curve. The Mo(V/IV) midpoint potential (Table 4) is similar to that of the *E. coli* Nar (*42*, *43*).

The *P. aerophilum* Nar is the first active nitrate reductase harboring a W cofactor. As previously shown, this enzyme can also accommodate Mo as the active site metal (*14*). To directly compare the properties of the W and Mo cofactors, we purified nitrate reductase from *P. aerophilum* membranes that harbored both Mo- and W-Nars. Both types of enzymes are present when cells are grown with a mixture of 1 μM WO_4^{2-} and 0.5 μM MoO_4^{2-}. Metal analysis of Nar purified from these membranes revealed the presence of both W and Mo in a 1:0.73 ratio; approximately 40% of this preparation did not contain either Mo or W when normalized to the Fe content.

EPR spectroscopy of the as isolated mixed W/Mo-Nar preparation revealed both W(V) and Mo(V) EPR signals, but their relative proportions were dependent on pH (Figure 4). At pH 6, W(V) is the main component, whereas at pH 8.5, the EPR signal is solely due to Mo(V). The Mo(V) signal is slightly rhombic, yielding a lower g anisotropy than the W(V). However, the averages of the three g values from the W(V) and Mo(V) species are very similar (Table 4). In contrast to W(V), the Mo(V) signal is not split, suggesting no or, alternatively, a weak magnetic interaction with a nearby proton that is not resolved in the EPR spectrum. The Mo(V) EPR signal is similar to that of the Mo(V) form of the *E. coli* Nar observed at high pH with respect to the lack of resolved proton superhyperfine splitting (*45*). Although the mixed W/Mo-Nar preparation contained more W, as determined by metal analysis, the amount of Mo stabilized in the (V) oxidation state (~35%) as visualized by EPR spectroscopy was significantly higher than the amount of the stabilized W(V) form (~11%) (Table 4). Quinol reduction and nitrate oxidation experiments as reported in Figure 3 for the pure W-Nar indicated a similar reversible redox behavior for both W(V) and Mo(V) in the mixed W/Mo-Nar preparation (data not shown). The mixed W/Mo-Nar preparation exhibited EPR properties of the [Fe-S] centers that were identical to those of the pure W-Nar, suggesting that the active site cofactor is inconsequential for the EPR spectra of the [Fe-S] centers (data not shown).

Redox Properties of NarGH Cofactors. To determine the midpoint potentials of the [Fe-S] centers and the W and Mo cofactors, dye-mediated redox titrations were performed with various purified W-Nar and W/Mo-Nar preparations at pH 6, 7, and 8. In contrast to single oxidation and reduction experiments using nitrate and plumbagin, dye-mediated redox titrations resulted in the complete loss of either W(V) or Mo(V) EPR signals. We attribute the loss of these EPR signals to the instability of both W and Mo cofactors in the detergent-solubilized enzyme, while the [Fe-S] centers remained stable (not shown). We, therefore, performed redox titrations with membranes isolated either from cells grown with 4.5 μM WO_4^{2-} and no added MoO_4^{2-} or from cells grown with a mixture of 1 μM WO_4^{2-} and 0.5 μM MoO_4^{2-}. EPR spectroscopy revealed a stable signal for Mo(V) but not for W(V) (see the bottom trace in Figure 4). The absence of a W(V) EPR signal indicates the relatively low stability of the W-Nar during redox titration experiments. The EPR signal of Mo(V) for membrane-associated Nar was unsplit but differed slightly in its g_z value from that obtained for the purified enzyme (g_z of 1.963 instead of 1.955). In membranes, the Mo(V) signal was present at both pH 6 and 8 with the same intensity.

Redox titrations at pH 6 and 8 of the Mo cofactor of membrane-associated Nar displayed a sigmoid rather than a bell-shaped curve (E_m = 88 mV) indicative of the Mo(V/IV) transition state only (Figure 5). This apparent stabilization of Mo(V) in the *P. aerophilum* Nar at high redox potentials points to a disequilibrium in which the Mo(V) cannot be further oxidized

to the Mo(VI) state. Such disequilibrium was also observed for the *E. coli* Nar at pH 6, but not at pH 8 (*45*). Because we could not determine the midpoint potential of the W(V/IV) redox couple using dye-mediated redox titrations, we estimated this value as -8 ± 15 mV based on the extent of reduction by PBH_2 at pH 6 (see Figure 3 and Table 3). Thus, the estimated midpoint potentials of the W(V/IV) and Mo(V/IV) redox couples differ by only approximately 100 mV.

The midpoint potentials for the [Fe-S] centers were determined using purified Nar (Figure 5) and are summarized in Table 3. The midpoint potentials of the [Fe-S] centers were generally found to be lower in the *P. aerophilum* Nar than those determined for the *E. coli* Nar (Table 3).

DISCUSSION

It has been somewhat of a conundrum how microbes maintain their ability to respire with nitrate using Mo-containing Nar in an environment that is naturally enriched with W (*21*). Generally, microbes adapt to their environmental metal content by expressing distinct enzymes, e.g., Mo- and W-formate dehydrogenases and Mo- and W-formylmethanofuran dehydrogenase in *Methanobacterium thermoautotrophicum* and *Methanobacterium wolfei* (*23*, *46*−*48*). Recently, several authors have demonstrated that W can replace Mo as the active site metal in the *E. coli* TMAO reductase, the *Desulfovibrio alaskensis* formate dehydrogenase, and the *Rhodobacter capsulatus* DMSO reductase (*49*−*51*). However, the membrane-bound NarGHI and the periplasmic Nap-type Nar were inactive with W (*22*, *43*, *52*). We report here the characterization of the first W-containing nitrate reductase isolated from the hyperthermophilic archaeon *P. aerophilum* grown with 4.5 μM WO_4^{2-}. The *P. aerophilum* W-Nar is identical to the previously described Mo-Nar, demonstrating that the type of metal cofactor is dependent on the environmental metal concentration (*14*). Thus, W can act effectively as an active site metal in more redox positive reactions [E_m°(nitrate/nitrite) = 420 mV] than originally assumed (*53*).

The Mo-Nar is twice as active as the W-Nar (Table 1), which is similar to the *E. coli* TMAO reductase, but in contrast to the *R. capsulatus* DMSO reductase (*14*, *50*, *51*); the W-substituted DMSO reductase was 17 times more active in the reduction of DMSO than the Mo-substituted enzyme (*51*). However, the W-substituted DMSO reductase was inactive in the reverse reaction, the oxidation of dimethyl sulfide (DMS) (*51*). This can be explained by the approximately 330 mV lower midpoint potential of the W(V/IV) redox couple as compared to the Mo(V/IV) couple (*54*). Interestingly, the midpoint potential of the W-Nar W(V/IV) redox couple is only approximately 100 mV lower than that of the Mo(V/IV) redox couple of the Mo-Nar (Table 3) and similar to that of the endogenous menaquinol. This suggests that the *P. aerophilum* Nar has evolved to efficiently utilize either metal cofactor, possibly as a reflection of steep temperature and metal ion gradients in their natural habitat. The reason why the *P. aerophilum* Nar can function with W as a metal cofactor whereas bacterial Nars cannot could be due to the successful coordination and retention of this metal within the NarG subunit. Why this might be so cannot, however, be easily explained because the primary ligands of the W and Mo cofactor (bis-dithiolene sulfur atoms and aspartate) are conserved with bacterial Nars. It is possible that the nature of second sphere ligands in *P. aerophilum* NarG contributes to the accommodation of either W or Mo as the active site metal. Alternatively, an altered NarG maturation pathway may allow for insertion of either W or Mo into the *P. aerophilum* Nar depending on the environmental concentrations of the two metals. Vergnes et al. showed that a Mo-bisMDG but not a W-bisMDG promoted an interaction among the Mo cofactor biosynthesis machinery, NarJ, and NarG, resulting in the successful incorporation of the Mo cofactor into the *E. coli* Nar (*55*). All three Mo cofactor biosynthesis proteins, MoeA, MobA, and MoaB (MogA in *E. coli*), that deliver the cofactor to NarG are conserved in *P. aerophilum*. We speculate that in *P. aerophilum* these homologues are adapted to allow for both W and Mo cofactor delivery.

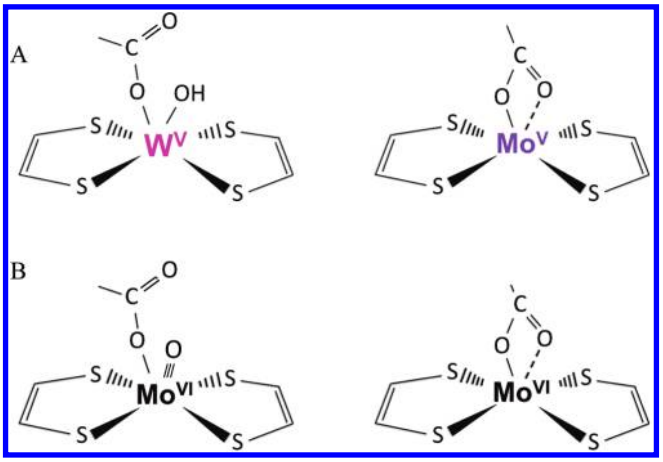

FIGURE 6: Proposed W(V)- and Mo(V)-Nar active site coordination of the *P. aerophilum* Nar. Metal coordination is based on EPR results obtained in this study (A) and on the mono- and bidentate coordination of Mo(VI) identified in the crystal structures of *E. coli* Nar (B) (*12*, *13*). Reduction of W(VI) to W(V) is accompanied by the binding of a proton to the oxo group, which becomes a hydroxo group. The oxo/hydroxo group is present at the metal center in the case of a monodentate coordination by Asp241. Reduction of the bidentate-coordinated Mo(VI) to Mo(V) in the *P. aerophilum* Nar does not lead to binding of an additional proton at or close to the Mo(V) (A). See the text for further explanation. The carboxyl groups in the drawing represent the side chain of Asp241 of *P. aerophilum* Nar (A) or Asp222 of *E. coli* Nar (B).

Reduction−oxidation experiments using reduced plumbagin and nitrate indicated reversible redox chemistry with both substrates at both the W and Mo active sites (Figure 3), indicating that the W(V) and Mo(V) EPR signals reflect genuine reaction intermediates. While the W(V) EPR signal is split because of proton superhyperfine interaction, the Mo(V) signal is unsplit, suggesting such interaction is absent or very weak. Somewhat surprising were the observations that with an increase in the pH of the solubilized mixed W/Mo-Nar enzyme preparation, the signal intensity of W(V) decreased, that of Mo(V) increased, while the line shape for both metal signals remained the same (Figure 4). This is in contrast to the *E. coli* Nar, in which Mo(V) undergoes a reversible change in protonation state with a pK_a of 7.4 as reflected in a change of split to unsplit EPR signal when the pH is increased above the pK_a (*45*). We, therefore, suggest that in the as isolated, partially reduced *P. aerophilum* Nar the change in pH leads to a new redox equilibrium of the various W and Mo redox states (Figure 6).

The finding that the W(V) is protonated whereas the Mo(V) is not suggests that in the *P. aerophilum* Nar the two metals occur in different ligation states. Crystal structures of the *E. coli* NarGHI and NarGH enzyme complexes show that Mo(VI) can be coordinated in a monodentate or bidentate manner by a conserved aspartate residue (Asp222 in *E. coli*) (*12*, *13*) (Figure 6B).

When Asp222 coordinates Mo(VI) as a monodentate ligand, an additional oxo group is bound to the Mo(VI). However, when Asp222 acts as a bidentate ligand, the oxo group is absent. This Asp residue is conserved in the *P. aerophilum* NarG sequence (Asp241) and is the likely ligand to the W and Mo cofactors in the *P. aerophilum* Nar.

When an oxo group is coordinated to W/Mo(VI) as in Nars, the subsequent reduction to W/Mo(V) leads to protonation of the oxo group to a hydroxo group (*43*). The OH proton of the hydroxo group is responsible for the proton superhyperfine interaction observed in EPR (see Figure 3) (*43*). Because in the W-Nar the W(V) EPR signal is split, we propose that W is coordinated in a monodentate fashion (Figure 6A). The lack of resolved proton superhyperfine splitting in the Mo(V) EPR spectrum indicates the absence of an oxo/hydroxo group and suggests a bidentate ligation by Asp241 for this metal (Figure 6A). Because in the *P. aerophilum* Nar, both W(V) and Mo(V) appear as genuine catalytic intermediates (Figures 3 and 4), both the mono- and bidentate ligations observed in the *E. coli* Mo-Nar crystals may in fact reveal two different catalytic intermediates.

EPR spectroscopy revealed that the [Fe-S] center properties of the *P. aerophilum* W- and Mo-Nar enzymes are identical. The *P. aerophilum* Nar [Fe-S] centers resemble closely those of the *E. coli* enzyme, exhibiting similar *g* values and magnetic complexity (*43*). The midpoint potentials of the *P. aerophilum* Nar [Fe-S] centers and heme o_P were determined by dye-mediated titrations (Table 3). Because purified Nar loses its W or Mo cofactor in these titrations, the values in Table 3 apply to the apo-Nar. The midpoint potentials determined for the [Fe-S] centers in the *P. aerophilum* Nar were generally much lower than those of the *E. coli* Mo-Nar (Table 3). We currently do not know whether this is due to the loss of the Mo or W cofactor in the dye-mediated redox titrations, a possible artifact caused by removal of lipids during purification (*43*), or whether this represents a true adaptation to service the more redox-negative W cofactor.

A striking difference between bacterial and archaeal Nars is their membrane anchor. All bacterial Nars contain a highly hydrophobic NarI subunit with five transmembrane helices and two *b*-type hemes (b_P and b_D) (*12*). In contrast, the archaeal Nars associate with a less hydrophobic NarM subunit containing two putative transmembrane helices, one located at the very N-terminus and a second at the very C-terminus of the protein. The *P. aerophilum* NarM peptide coordinates only one heme of the o_P type similar to the o_P hemes of the *P. aerophilum* NO reductase described previously (*56*). The g_z value (3.31) of the rhombic heme o_P EPR signal is similar to that of the low-spin heme *b* (g_z = 3.33) in SerC, the γ subunit of the periplasmic selenate reductase from *T. selenatis* (*57*). Archaeal NarMs are distantly related to SerC and the γ subunit of the periplasmic ethylbenzene dehydrogenase, EbdC, from *A. aromaticum* strain EbN1, which was recently crystallized by Kloer et al. (Figure 1B) (*30*). The Ebd crystal structure demonstrates that Fe(III) of heme *b* is coordinated by Met108 and Lys201 (*A. aromaticum*), which are conserved in SerC, all other bacterial homologues, and all NarM family members and are, thus, the likely ligands to the heme o_P Fe(III) of *P. aerophilum* NarM (*18*). On the basis of the outward orientation of Nar and the resemblance of NarM to the γ subunits of selenate reductase and ethylbenzene dehydrogenase, we envision that archaeal Nars may present evolutionary precursors to diversified bacterial periplasmic oxidoreductase enzymes catalyzing reactions with end products such as nitrite and selenite, which are harmful to the cell's interior (*58*).

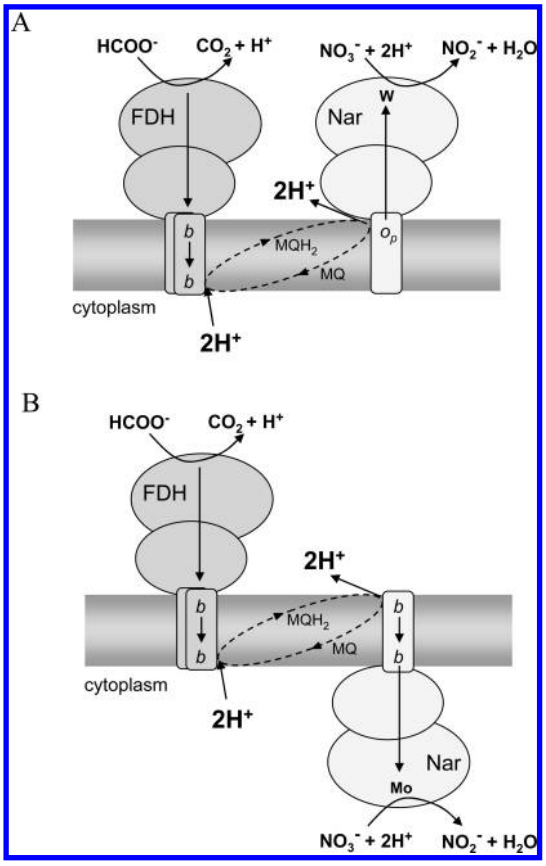

FIGURE 7: Bioenergetic consequence of the cellular orientation of archaeal and bacterial Nars. In archaea, Nar is oriented toward the cell's exterior (*18*) (A). As a consequence, Nar receives its electrons and protons at the same face of the cytoplasmic membrane and is as such electro-neutral. In bacteria (B), the inward-oriented Nar receives electrons on the periplasmic side from MQH_2. The bacterial Nar contains two hemes in a transmembrane arrangement allowing electrogenic transmembrane electron transfer. As a consequence, in bacteria, Nar contributes to the pmf. Arrows indicate electron flow. FDH denotes membrane-bound formate dehydrogenase that reduces menaquinone.

The presence of only one heme in NarM is consistent with the experimentally determined outward orientation of *P. aerophilum*, *H. marismortui*, and *Ha. mediterranei* Nars (Figure 7A) (*16*, *18*). We expect that the single heme in NarM must be located close to both the quinone binding site and FS4 to facilitate electron transfer. The presence of a Tat motif, consisting of a signal peptide with a twin-arginine motif, in all archaeal NarG N-termini suggests that an outward orientation appears to be an archaeal commonality (*18*). The Tat translocon serves to transport folded proteins, often containing cofactors, across the cytoplasmic membrane to the periplasmic compartment of Gram-negative bacteria or the exterior space in Gram-positive bacteria and archaea (*59*−*61*).

As noted by Turner et al. (*34*), a sequence reminiscent of the Tat motif is still recognizable in N-termini of bacterial NarG subunits, supporting the notion that the bacterial NarGHI complex may have evolved from an enzyme with a periplasmic orientation. Through mutagenesis, the *E. coli* NarG N-terminus could be converted into a Tat transport competent signal peptide albeit at the expense of proper NarGH assembly (*61*). Because the Tat translocon accepts only fully folded proteins, many cofactor-associated oxidoreductases require private "Tat-proofreading chaperones" that protect their enzyme from Tat transport rejection and aid in enzyme maturation (*60*). NarGHI depends on the

NarJ chaperone, which has been demonstrated to bind to the N-terminus of NarG and exhibits multifunctional roles in maturation and assembly of the NarGHI complex (*33*). NarJ belongs to the TorD family of redox enzyme maturation proteins (REMP), most of which chaperone redox enzymes for cellular export to the Tat translocon machinery (*34*).

The cellular arrangement of Nar presents archaea with a potential bioenergetic disadvantage as an outward-oriented Nar does not contribute directly to the generation of the proton motive force (Figure 7A). In contrast, the cytoplasmic orientation of bacterial Nars with their transmembrane arrangement of the two hemes provides a vectorial component enabling the generation of a pmf (Figure 7B). Thus, in *P. aerophilum*, neither Nar nor the other denitrification enzymes generate a pmf because they are quinone-linked with an outward orientation (*7*). When nitrate respiration is linked to the oxidation of formate, a pmf will be established by the formate dehydrogenase (Figure 7A). The haloarchaea *H. marismortui* and *Ha. mediterranei* may have evolved a more efficient mode of nitrate respiration by receiving electrons directly from an electrogenic bc_1 complex as proposed by Yoshimatsu et al. and Martinez-Espinosa et al. (*18*, *20*). While genes for a bc_1-type complex are present in the *P. aerophilum* genome, the specific EPR signal of the Rieske-type Fe−S protein associated with an active bc_1-type complex could not be detected in membranes of *P. aerophilum* grown under denitrifying conditions (S. de Vries, personal communication) (*7*) . The question of why Nars in archaea assume this seemingly unfavorable cellular orientation arises. We speculate that Nars may have evolved in hot environments similar to those that are inhabited by hyperthermophiles such as *P. aerophilum* (*62*). Given that in hot habitats *N*-oxide toxicity is accelerated, an outward orientation may constitute a protective mechanism shared by all consecutive denitrification pathway enzymes (*11*). Thus, we suggest that the four denitrification enzymes may have evolved to serve as an electron sink assuming outward-facing orientations shielding the cell from the reactive *N*-oxides. The presence of a W cofactor may be reflective of an often higher concentration of this metal at high temperatures (*21*). Bacterial Mo-Nars assuming a cytoplasmic orientation could have evolved at lower temperatures as a result of a Tat motif mutation disabling transmembrane protein translocation via the Tat translocation machinery (*59*, *60*). We suggest that the NarI membrane anchor coordinating a second heme for transmembrane electron transport evolved as an efficient bioenergetic addition (Figure 7B). The cytoplasmic orientation of bacterial Nars necessitates the simultaneous evolution of a NarK-type nitrate/nitrite transporter, which is absent from *Pyrobaculum* genomes.

SUPPORTING INFORMATION AVAILABLE

A method for heme identification by size exclusion chromatography and electrospray ionization mass spectrometry (SEC−MS), redox titration of the hemes, and purification table for Nar. This material is available free of charge via the Internet at http://pubs.acs.org.

REFERENCES

1. Zumft, W. G., and Körner, H. (1997) Enzyme diversity and mosaic gene organization in denitrification. *Antonie van Leeuwenhoek 71*, 43–58.
2. Wasser, I. M., de Vries, S., Moenne-Loccoz, P., Schröder, I., and Karlin, K. D. (2002) Nitric oxide in biological denitrification: Fe/Cu metalloenzyme and metal complex NOx redox chemistry. *Chem. Rev. 102*, 1201–1234.
3. Richardson, D. J., and Watmough, N. J. (1999) Inorganic nitrogen metabolism in bacteria. *Curr. Opin. Chem. Biol. 3*, 207–219.
4. Schröder, I., and de Vries, S. (2008) Respiratory Pathways in Archaea. In Archaea: New models for prokaryotic biology (Blum, P., Ed.) pp 1−26, Caister Academic Press, Norwich, U.K.
5. de Vries, S., and Schröder, I. (2007) Denitrification pathway enzymes of thermophiles. In Thermophiles: Biology and Technology at High Temperature (Robb, F., Antranikian, G., Grogan, D., and Driessen, A., Eds.) CRC Press, Boca Raton, FL.
6. Afshar, S., Kim, C., Monbouquette, H. G., and Schröder, I. (1998) Effect of tungstate on nitrate reduction by the hyperthermophilic archaeon *Pyrobaculum aerophilum*. *Appl. Environ. Microbiol. 64*, 3004–3008.
7. de Vries, S., and Schröder, I. (2002) Comparison between the nitric oxide reductase family and its aerobic relatives, the cytochrome oxidases. *Biochem. Soc. Trans. 30*, 662–667.
8. Suharti, Strampraad, M. J. F., Schröder, I., and de Vries, S. (2001) A novel copper A containing menaquinol NO reductase from *Bacillus azotoformans*. *Biochemistry 40*, 2632–2639.
9. Philippot, L. (2002) Denitrifying genes in bacterial and archaeal genomes. *Biochim. Biophys. Acta 1577*, 355–376.
10. Richardson, D. J., Berks, B. C., Russell, D. A., Spiro, S., and Taylor, C. J. (2001) Functional, biochemical and genetic diversity of prokaryotic nitrate reductases. *Cell. Mol. Life Sci. 58*, 165–178.
11. Zumft, W. G. (1997) Cell biology and molecular basis of denitrification. *Microbiol. Mol. Biol. Rev. 61*, 533–616.
12. Bertero, M. G., Rothery, R. A., Palak, M., Hou, C., Lim, D., Blasco, F., Weiner, J. H., and Strynadka, N. C. (2003) Insights into the respiratory electron transfer pathway from the structure of nitrate reductase A. *Nat. Struct. Biol. 10*, 681–687.
13. Jormakka, M., Richardson, D., Byrne, B., and Iwata, S. (2004) Architecture of NarGH reveals a structural classification of Mo-bis-MGD enzymes. *Structure 12*, 95–104.
14. Afshar, S., Johnson, E., de Vries, S., and Schröder, I. (2001) Properties of a thermostable nitrate reductase from the hyperthermophilic archaeon *Pyrobaculum aerophilum*. *J. Bacteriol. 183*, 5491–5495.
15. Martinez-Espinosa, R. M., Richardson, D. J., Butt, J. N., and Bonete, M. J. (2006) Respiratory nitrate and nitrite pathway in the denitrifier haloarchaeon *Haloferax mediterranei*. *Biochem. Soc. Trans. 34*, 115–117.
16. Yoshimatsu, K., Iwasaki, T., and Fujiwara, T. (2002) Sequence and electron paramagnetic resonance analyses of nitrate reductase NarGH from a denitrifying halophilic euryarchaeote *Haloarcula marismortui*. *FEBS Lett. 516*, 145–150.
17. Yoshimatsu, K., Sakurai, T., and Fujiwara, T. (2000) Purification and characterization of dissimilatory nitrate reductase from a denitrifying halophilic archaeon, *Haloarcula marismortui*. *FEBS Lett. 470*, 216–220.
18. Martinez-Espinosa, R. M., Dridge, E. J., Bonete, M. J., Butt, J. N., Butler, C. S., Sargent, F., and Richardson, D. J. (2007) Look on the positive side! The orientation, identification and bioenergetics of 'Archaeal' membrane-bound nitrate reductases. *FEMS Microbiol. Lett. 276*, 129–139.
19. Richardson, D. J. (2000) Bacterial respiration: A flexible process for a changing environment. *Microbiology 146*, 551–571.
20. Yoshimatsu, K., Araya, O., and Fujiwara, T. (2007) *Haloarcula marismortui* cytochrome b_{-561} is encoded by the *narC* gene in the dissimilatory nitrate reductase operon. *Extremophiles 11*, 41–47.
21. Klenitz, A., and Adams, M. W. W. (1996) Tungsten in biological systems. *FEMS Microbiol. Rev. 18*, 5–63.
22. Gates, A. J., Hughes, R. O., Sharp, S. R., Millington, P. D., Nilavongse, A., Cole, J. A., Leach, E. R., Jepson, B., Richardson, D. J., and Butler, C. S. (2003) Properties of the periplasmic nitrate reductases from *Paracoccus pantotrophus* and *Escherichia coli* after growth in tungsten-supplemented media. *FEMS Microbiol. Lett. 220*, 261–269.
23. Moura, J. J., Brondino, C. D., Trincao, J., and Romao, M. J. (2004) Mo and W bis-MGD enzymes: Nitrate reductases and formate dehydrogenases. *J. Biol. Inorg. Chem. 9*, 791–799.
24. Gunsalus, R. P., Cecchini, G., and Schröder, I. (2007) Bacterial Respiration, 3rd ed., ASM Press, Washington, DC.
25. Hilton, J. C., and Rajagopalan, K. V. (1996) Identification of the molybdenum cofactor of dimethyl sulfoxide reductase from *Rhodobacter sphaeroides* f. sp. *denitrificans* as bis(molybdopterin guanine dinucleotide)molybdenum. *Arch. Biochem. Biophys. 325*, 139–143.
26. Shevchenko, A., Wilm, M., Vorm, O., and Mann, M. (1996) Mass spectrometric sequencing of proteins silver-stained polyacrylamide gels. *Anal. Chem. 68*, 850–858.
27. Lübben, M., and Morand, K. (1994) Novel prenylated hemes as cofactors of cytochrome oxidases. Archaea have modified hemes A and O. *J. Biol. Chem. 269*, 21473–21479.

28. Whitelegge, J. P., le Coutre, J., Lee, J. C., Engel, C. K., Prive, G. G., Faull, K. F., and Kaback, H. R. (1999) Toward the bilayer proteome, electrospray ionization-mass spectrometry of large, intact transmembrane proteins. *Proc. Natl. Acad. Sci. U.S.A. 96*, 10695–10698.
29. von Wachenfeldt, C., de Vries, S., and van der Oost, J. (1994) The CuAsite of the caa3-type oxidase of *Bacillus subtilis* is a mixed-valence binuclear copper centre. *FEBS Lett. 340*, 109–113.
30. Kloer, D. P., Hagel, C., Heider, J., and Schulz, G. E. (2006) Crystal structure of ethylbenzene dehydrogenase from *Aromatoleum aromaticum*. *Structure 14*, 1377–1388.
31. Kniemeyer, O., and Heider, J. (2001) Ethylbenzene dehydrogenase, a novel hydrocarbon-oxidizing molybdenum/iron-sulfur/heme enzyme. *J. Biol. Chem. 276*, 21381–21386.
32. Krafft, T., Bowen, A., Theis, F., and Macy, J. M. (2000) Cloning and sequencing of the genes encoding the periplasmic-cytochrome B-containing selenate reductase of *Thauera selenatis*. *DNA Sequence 10*, 365–377.
33. Lanciano, P., Vergnes, A., Grimaldi, S., Guigliarelli, B., and Magalon, A. (2007) Biogenesis of a respiratory complex is orchestrated by a single accessory protein. *J. Biol. Chem. 282*, 17468–17474.
34. Turner, R. J., Papish, A. L., and Sargent, F. (2004) Sequence analysis of bacterial redox enzyme maturation proteins (REMPs). *Can. J. Microbiol. 50*, 225–238.
35. Vergnes, A., Pommier, J., Toci, R., Blasco, F., Giordano, G., and Magalon, A. (2006) NarJ chaperone binds on two distinct sites of the aponitrate reductase of *Escherichia coli* to coordinate molybdenum cofactor insertion and assembly. *J. Biol. Chem. 281*, 2170–2176.
36. Hille, R. (2002) Molybdenum and tungsten in biology. *Trends Biochem. Sci. 27*, 360.
37. Schwarz, G., Mendel, R. R., and Ribbe, M. W. (2009) Molybdenum cofactors, enzymes and pathways. *Nature 460*, 839–847.
38. Kroger, A., Dorrer, E., and Winkler, E. (1980) The orientation of the substrate sites of formate dehydrogenase and fumarate reductase in the membrane of *Vibrio succinogenes*. *Biochim. Biophys. Acta 589*, 118–136.
39. Magalon, A., Lemesle-Meunier, D., Rothery, R. A., Frixon, C., Weiner, J. H., and Blasco, F. (1997) Heme axial ligation by the highly conserved His residues in helix II of cytochrome *b* (NarI) of *Escherichia coli* nitrate reductase A. *J. Biol. Chem. 272*, 25652–25658.
40. Bertero, M. G., Rothery, R. A., Boroumand, N., Palak, M., Blasco, F., Ginet, N., Weiner, J. H., and Strynadka, N. C. (2005) Structural and biochemical characterization of a quinol binding site of *Escherichia coli* nitrate reductase A. *J. Biol. Chem. 280*, 14836–14843.
41. Blasco, F., Guigliarelli, B., Magalon, A., Asso, M., Giordano, G., and Rothery, R. A. (2001) The coordination and function of the redox centres of the membrane-bound nitrate reductases. *Cell. Mol. Life Sci. 58*, 179–193.
42. Guigliarelli, B., Asso, M., More, C., Augier, V., Blasco, F., Pommier, J., Giordano, G., and Bertrand, P. (1992) EPR and redox characterization of iron-sulfur centers in nitrate reductases A and Z from *Escherichia coli*. Evidence for a high-potential and a low-potential class and their relevance in the electron-transfer mechanism. *Eur. J. Biochem. 207*, 61–68.
43. Rothery, R. A., Magalon, A., Giordano, G., Guigliarelli, B., Blasco, F., and Weiner, J. H. (1998) The molybdenum cofactor of *Escherichia coli* nitrate reductase A (NarGHI). Effect of a *mobAB* mutation and interactions with [Fe-S] clusters. *J. Biol. Chem. 273*, 7462–7469.
44. Rothery, R. A., Bertero, M. G., Cammack, R., Palak, M., Blasco, F., Strynadka, N. C., and Weiner, J. H. (2004) The catalytic subunit of *Escherichia coli* nitrate reductase A contains a novel [4Fe-4S] cluster with a high-spin ground state. *Biochemistry 43*, 5324–5333.
45. Magalon, A., Asso, M., Guigliarelli, B., Rothery, R. A., Bertrand, P., Giordano, G., and Blasco, F. (1998) Molybdenum cofactor properties and [Fe-S] cluster coordination in *Escherichia coli* nitrate reductase A: Investigation by site-directed mutagenesis of the conserved his-50 residue in the NarG subunit. *Biochemistry 37*, 7363–7370.
46. Schmitz, R. A., Richter, M., Linder, D., and Thauer, R. K. (1992) A tungsten-containing active formylmethanofuran dehydrogenase in the thermophilic archaeon *Methanobacterium wolfei*. *Eur. J. Biochem. 207*, 559–565.
47. Bertram, P. A., Schmitz, R. A., Linder, D., and Thauer, R. K. (1994) Tungstate can substitute for molybdate in sustaining growth of *Methanobacterium thermoautotrophicum*. Identification and characterization of a tungsten isoenzyme of formylmethanofuran dehydrogenase. *Arch. Microbiol. 161*, 220–228.
48. Hochheimer, A., Hedderich, R., and Thauer, R. K. (1998) The formylmethanofuran dehydrogenase isoenzymes in *Methanobacterium wolfei* and *Methanobacterium thermoautotrophicum*: Induction of the molybdenum isoenzyme by molybdate and constitutive synthesis of the tungsten isoenzyme. *Arch. Microbiol. 170*, 389–393.
49. Brondino, C. D., Passeggi, M. C., Caldeira, J., Almendra, M. J., Feio, M. J., Moura, J. J., and Moura, I. (2004) Incorporation of either molybdenum or tungsten into from *Desulfovibrio alaskensis* NCIMB 13491; EPR assignment of the proximal iron-sulfur cluster to the pterin cofactor in formate dehydrogenases from sulfate-reducing bacteria. *J. Biol. Inorg. Chem. 9*, 145–151.
50. Buc, J., Santini, C. L., Giordani, R., Czjzek, M., Wu, L. F., and Giordano, G. (1999) Enzymatic and physiological properties of the tungsten-substituted molybdenum TMAO reductase from *Escherichia coli*. *Mol. Microbiol. 32*, 159–168.
51. Stewart, L. J., Bailey, S., Bennett, B., Charnock, J. M., Garner, C. D., and McAlpine, A. S. (2000) Dimethylsulfoxide reductase: An enzyme capable of catalysis with either molybdenum or tungsten at the active site. *J. Mol. Biol. 299*, 593–600.
52. Amy, N. K., and Rajagopalan, K. V. (1979) Characterization of molybdenum cofactor from *Escherichia coli*. *J. Bacteriol. 140*, 114–124.
53. Johnson, M. K., Rees, D. C., and Adams, M. W. (1996) Tungstoenzymes. *Chem. Rev. 96*, 2817–2840.
54. Hagedoorn, P. L., Hagen, W. R., Stewart, L. J., Docrat, A., Bailey, S., and Garner, C. D. (2003) Redox characteristics of the tungsten DMSO reductase of *Rhodobacter capsulatus*. *FEBS Lett. 555*, 606–610.
55. Vergnes, A., Gouffi-Belhabich, K., Blasco, F., Giordano, G., and Magalon, A. (2004) Involvement of the molybdenum cofactor biosynthetic machinery in the maturation of the *Escherichia coli* nitrate reductase A. *J. Biol. Chem. 279*, 41398–41403.
56. de Vries, S., Strampraad, M. J., Lu, S., Moenne-Loccoz, P., and Schröder, I. (2003) Purification and characterization of the MQH2: NO oxidoreductase (qNOR) from the hyperthermophilic Archaeon *Pyrobaculum aerophilum*. *J. Biol. Chem. 278*, 35861–35868.
57. Dridge, E. J., Watts, C. A., Jepson, B. J., Line, K., Santini, J. M., Richardson, D. J., and Butler, C. S. (2007) Investigation of the redox centres of periplasmic selenate reductase from *Thauera selenatis* by EPR spectroscopy. *Biochem. J. 408*, 19–28.
58. Watts, C. A., Ridley, H., Dridge, E. J., Leaver, J. T., Reilly, A. J., Richardson, D. J., and Butler, C. S. (2005) Microbial reduction of selenate and nitrate: Common themes and variations. *Biochem. Soc. Trans. 33*, 173–175.
59. Palmer, T., Sargent, F., and Berks, B. C. (2005) Export of complex cofactor-containing proteins by the bacterial Tat pathway. *Trends Microbiol. 13*, 175–180.
60. Sargent, F. (2007) The twin-arginine transport system: Moving folded proteins across membranes. *Biochem. Soc. Trans. 35*, 835–847.
61. Ize, B., Coulthurst, S. J., Hatzixanthis, K., Caldelari, I., Buchanan, G., Barclay, E. C., Richardson, D. J., Palmer, T., and Sargent, F. (2009) Remnant signal peptides on non-exported enzymes: Implications for the evolution of prokaryotic respiratory chains. *Microbiology 155*, 3992–4004.
62. Völkl, P., Huber, R., Drobner, E., Rachel, R., Burggraf, S., Trincone, A., and Stetter, K. O. (1993) *Pyrobaculum aerophilum* sp. nov., a novel nitrate reducing hyperthermophilic Archaeum. *Appl. Environ. Microbiol. 59*, 2918–2926.
63. Rothery, R. A., Blasco, F., Magalon, A., Asso, M., and Weiner, J. H. (1999) The hemes of *Escherichia coli* nitrate reductase A (NarGHI): Potentiometric effects of inhibitor binding to narI. *Biochemistry 38*, 12747–12757.
64. Magalon, A., Rothery, R. A., Giordano, G., Blasco, F., and Weiner, J. H. (1997) Characterization by electron paramagnetic resonance of the role of the *Escherichia coli* nitrate reductase (NarGHI) iron-sulfur clusters in electron transfer to nitrate and identification of a semiquinone radical intermediate. *J. Bacteriol. 179*, 5037–5045.